Mid-infrared Integrated Electro-optic Modulator Operating up to 225 MHz between 6.4 and 10.7 μm Wavelength

Miguel Montesinos-Ballester, Lucas Deniel, Natnicha Koompai, Thi Hao Nhi Nguyen, Jacopo Frigerio, Andrea Ballabio, Virginia Falcone, Xavier Le Roux, Carlos Alonso-Ramos, Laurent Vivien, et al.

ACS Photonics

pubs.acs.org/journal/apchd5

Article

Mid-infrared Integrated Electro-optic Modulator Operating up to 225 MHz between 6.4 and 10.7 μm Wavelength

Miguel Montesinos-Ballester,* Lucas Deniel, Natnicha Koompai, Thi Hao Nhi Nguyen, Jacopo Frigerio, Andrea Ballabio, Virginia Falcone, Xavier Le Roux, Carlos Alonso-Ramos, Laurent Vivien, Adel Bousseksou, Giovanni Isella, and Delphine Marris-Morini

Cite This: https://doi.org/10.1021/acsphotonics.1c01449

Read Online

ACCESS | Metrics & More | Article Recommendations

ABSTRACT: Mid-infrared spectroscopy is essential for identifying molecular species, while related electro-optic modulators are crucial for signal-to-noise enhancement via synchronous detection. Therefore, the development of integrated modulators is expected to have a major impact in compact and widespread sensing applications. In this work, we experimentally demonstrate a broadband integrated electro-optic modulator, based on a graded-index SiGe photonics platform and free-carrier plasma dispersion effect. Optical modulation is reported from 6.4 to 10.7 μm wavelength, showing an operational frequency up to 225 MHz. These results pave the way for the development of multimolecule on-chip spectroscopic systems, operating at the longest mid-infrared wavelengths.

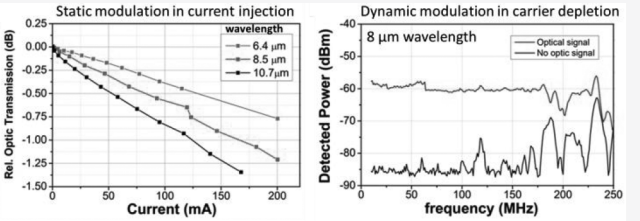

KEYWORDS: *mid-infrared, integrated photonic circuits, integrated modulator, silicon photonics, germanium, free-carrier plasma dispersion effect*

Spectroscopy sensing in the mid-infrared (mid-IR) range (2−20 μm wavelength) is an unambiguous way to detect and quantify small traces of environmental and toxic vapors. Mid-IR spectroscopy is thus exploited in a plethora of applications, including environment, defense, security, and industrial monitoring. However, current mid-IR devices are often based on a free-space configuration, thus becoming bulky and expensive. Therefore, the on-chip integration of spectroscopic systems would have a major impact in the development of efficient, portable and widespread sensing detectors. In particular, the wavelengths between 5 and 12 μm are of high interest, as many important molecules for pollution monitoring or healthcare (e.g., ozone or alkanes) have strong absorption lines in this spectral band. Hence, integrated electro-optic modulators (EOM) operating in this wavelength range would be essential for sensitivity enhancement via synchronous detection.[1] Furthermore, the mid-IR range contains two atmospheric transparency windows (i.e., 3−5 and 8−14 μm),[2] in which the development of high-speed optical modulators would also have a great impact on free-space communication applications,[3,4] among others.

In this regard, the development of integrated and efficient EOMs operating in a wide mid-IR spectral band, and particularly between 5 and 12 μm, would open exciting perspectives for multimolecule detection systems. However, its implementation remains challenging. For instance, intersubband transitions in III−V material quantum well structures have been exploited, as recently reported at 10 μm wavelength based on a free-space configuration.[5] Nevertheless, narrowband operation is intrinsically given by the heterostructure design. Alternatively, free-carrier plasma dispersion (FCPD) effect is a strong candidate for the realization of broadband modulator devices. In fact, silicon-on-insulator (SOI)-based EOMs exploiting the FCPD effect have been largely developed in the near-infrared range, and its operation has been recently extended up to 3.8 μm wavelength.[6,7] Interestingly, the magnitude of refractive index and absorption coefficient variation by FCPD increases at longer wavelengths. However, SOI waveguides show a transparency limit that prevents further wavelength extensions by mean of this type of platforms.

In parallel, germanium (Ge) and silicon−germanium (SiGe) alloys have shown a great potential for mid-IR photonics circuits, due to the wide transparency window of Ge (up to 15 μm wavelength).[3,7−9] Indeed, a whole set of passive building blocks have been developed by mean of different Ge and SiGe-

Received: September 21, 2021

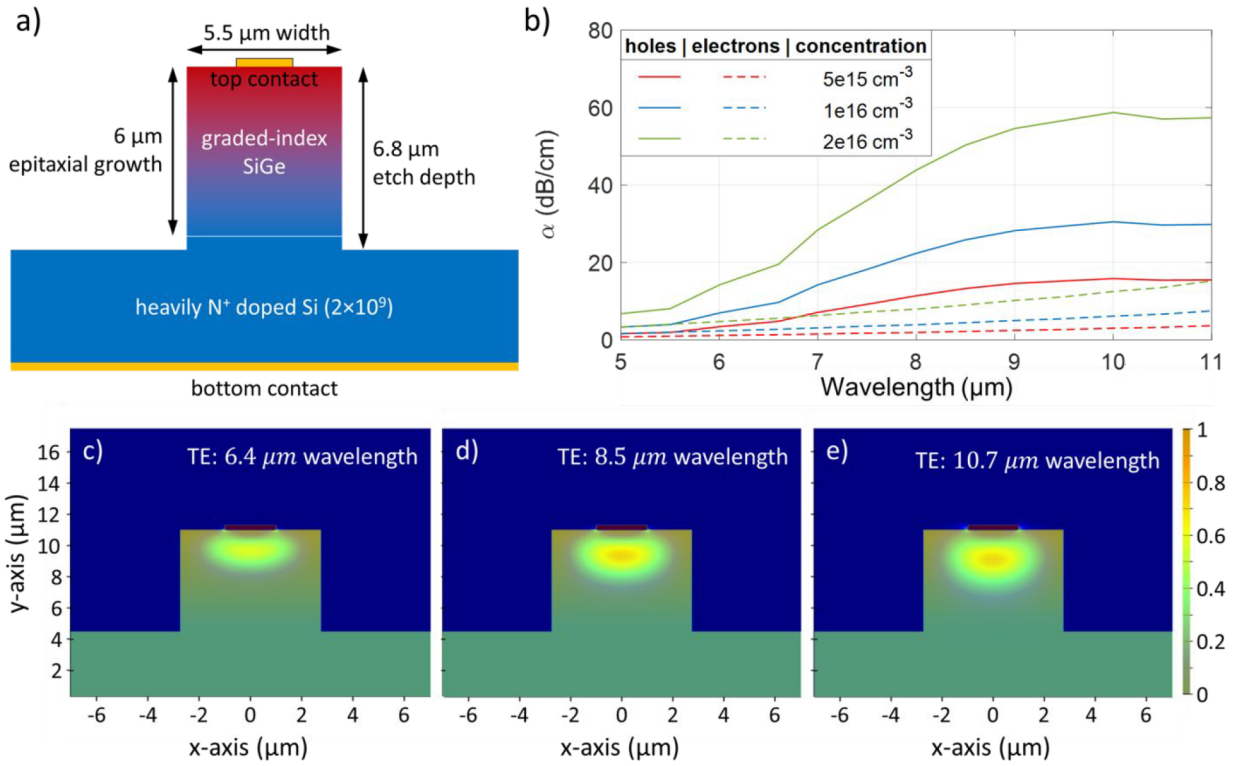

Figure 1. (a) Cut-view schematic of the EOM device. (b) Modeling of the absorption variation in bulk Ge as a function of the wavelength and for selected carrier concentrations.[19,22] Solid and dashed lines represent holes and electron concentrations, respectively. (c–e) Simulation of the fundamental TE mode profile at 6.4, 8.5, and 10.7 μm wavelengths. Scale bar: relative optical intensity.

based platforms.[10−17] Nevertheless, the development of efficient Ge or SiGe optical modulators in the long-wave part of the mid-IR spectrum is still at its infancy. Only one demonstration based on a PIN diode embedded in a Ge-on-Si waveguide has been reported, operating at 3.8 μm wavelength and demonstrating up to 60 MHz on−off keying modulation.[18] Also in that work, a preliminary electro-absorption modulation at 8 μm was shown. However, reaching efficient EOMs by FCPD effect in the long wavelength part of the mid-IR spectrum is challenging, mainly due to the increasing size of the optical mode profile at those wavelengths. On one hand, a larger optical mode leads to a reduction of its overlap with the fixed-size region in which the free-carrier concentration varies, thus limiting the modulation efficiency. On the other hand, modulators based of FCPD typically require highly doped layers. Therefore, a larger optical mode also leads to a higher overlap with those doped layers, thus increasing the optical losses of the device. In order to avoid this effect, the doped layers must be placed further away from the waveguide core, which may also limit the maximum modulation speed due to a higher access resistance.

In this work, a Ge-rich SiGe graded-index platform is proposed to demonstrate a broadband integrated EOM in the mid-IR. These kinds of platforms have already shown compelling results, such as all-optical modulation up to 11 μm wavelength[19] or two-octave supercontinuum generation in the mid-IR region.[20] Interestingly, we exploit the unique guiding properties of the graded SiGe waveguides to mitigate the above cited challenges. Indeed, unlike other kind of platforms (such as constant composition waveguides), the graded refractive index profile allows a broadband mode confinement on the top of the waveguide, where the carrier concentration variation is obtained by a Schottky diode. Also, a reduced overlap with a highly doped Si-substrate used to enable the electrical contact from the backside of the sample is achieved. Therefore, electro-optical modulation is achieved in a wide wavelength range, spanning from 6.4 to 10.7 μm. Noticeably, a maximum variation of 1.3 dB is achieved at 10.7 μm wavelength in injection regime, which is, to date, the largest electro-optical modulation reported on-chip at wavelengths longer than 8 μm. Also, a remarkably 225 MHz modulation speed is obtained in depletion regime, which is already compatible with the requirements of synchronous detection for signal-to-noise enhancement in spectroscopic detection systems. In summary, this work is the first experimental demonstration of broadband electro-optical modulation in mid-IR photonics integrated circuits, reaching wavelengths up to 10.7 μm.

RESULTS AND DISCUSSION

Modulator Design. The EOM device relies on a graded-index platform previously reported,[21] in which the Ge-concentration linearly increases from Si to Ge through a 6-μm-thick layer. This platform shows a good balance between optical propagation loss at the longest mid-IR wavelengths and compactness, which is required to achieve a fast and efficient modulator. To exploit the FCPD effect driven by an electrical signal, a vertical diode is considered. The bottom diode contact is obtained by depositing a metal layer on the back side of a highly n-type doped 500-μm-thick Si substrate. The top contact is formed by a metal strip deposited on top of the waveguide (Figure 1a). This configuration has been closed due to its fabrication simplicity (only two lithography steps, one dry etching step, and no ion implantation required).

https://doi.org/10.1021/acsphotonics.1c01449
ACS Photonics XXXX, XXX, XXX−XXX

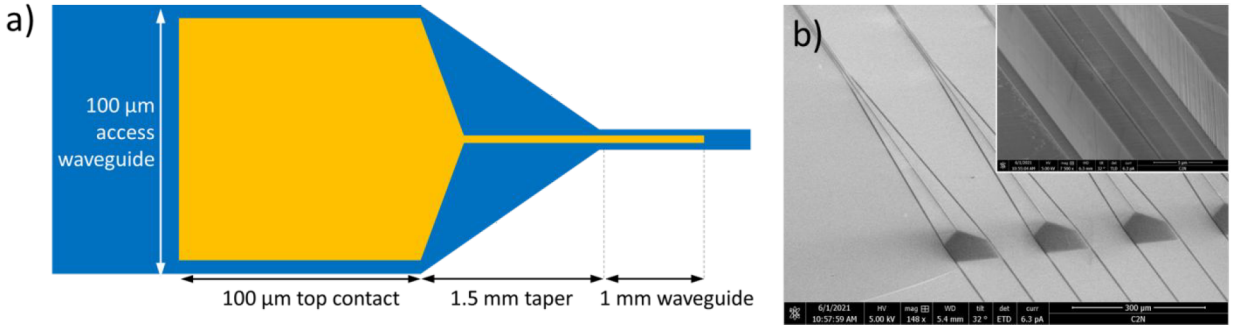

Figure 2. (a) Scale-less schematic top-view of the EOM. The 100-μm-width input access waveguide and the 96-μm-width top metal narrow down to the 5.5-μm-width waveguide and 2-μm-width top contact, respectively. The waveguide and the contacts are tapered along the 1.5 mm and 100 μm transitions, respectively. (b) Scanning electron microscope (SEM) image of the modulator. Inset: SEM image of the 5.5 μm-width waveguide section.

Numerical calculations of the optical mode profile are reported in Figure 1c–e for three different wavelengths (i.e., 6.4, 8.5, and 10.7 μm), considering a top metal rib of 300 nm thickness. The waveguide width is 5.5 μm and the etching depth is 6.8 μm. As observed in the mode calculations, the light is confined in the upper part of the waveguide. Also, as TM mode suffers from high losses because of the presence of the top metal, only TE polarization has been considered in this work.

Thanks to the vertical diode embedded in the waveguide, free-carrier variations are obtained by applying a bias voltage between the top and bottom electrodes. This carrier variations are then responsible for a modulation of the refractive index and absorption coefficient of the waveguide. In this work, straight waveguides are considered, thus the EOM will exploit only absorption modulation. The absorption coefficient spectra of different free-carrier concentrations are shown in Figure 1b, as reported in refs 19 and 22. As observed in this figure, the absorption coefficient by FCPD increases with the carrier concentration and wavelength, and this effect is stronger for holes (continuous lines) than for electrons (dash lines).

Sample Fabrication. The 6-μm-thick graded layer is epitaxially grown on top of a n-type doped Si substrate (As doping concentration of 2×10^{19} cm^{-3}) by low-energy plasma-enhanced chemical vapor deposition (LEPECVD), at a rate of 5–10 nm/s and using GeH_4 and SiH_4 as gas precursors.[23] Then, a metal strip is deposited on the sample surface, composed by a 10-nm-thickness of titanium and 300 nm of gold. The optical waveguides are then patterned in a lithography step, and ICP-RIE dry etching is used to define 6.8-μm-height structures. Finally, the bottom contact is obtained by depositing similar metal layers (10 nm of Ti and 300 nm pf Au) on the entire sample backside.

To allow a top probe contact and an efficient optical injection, the top metal is deposited over a fraction (100 μm of length) of a 100-μm-width input waveguide. As shown in Figure 2, the input waveguide is then tapered down to a 5.5-μm width over a 1.5-mm-length transition. The top metal strip is also extended through the taper transition and continued along a 1 mm section of the 5.5-μm-width waveguide. The final EOM device comprises a total waveguide length of 2.6 mm.

Electrical Characteristics and Propagation Losses. The measured I–V curve of the diode is reported in Figure 3. As both the substrate and the graded SiGe layer are n-type doped (as measured by hot-probe method[24]) this curve indicates that a Schottky barrier is obtained at the interface

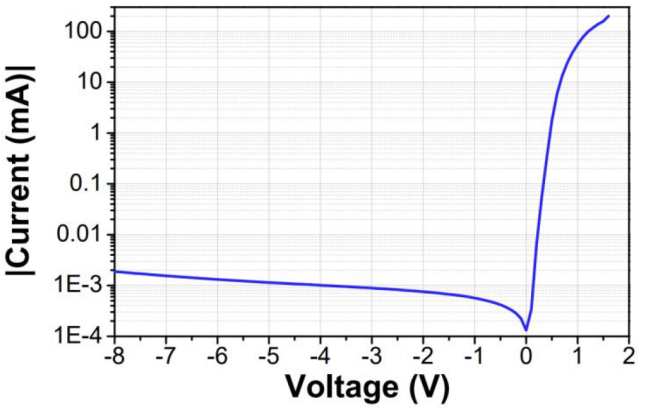

Figure 3. Absolute value of the current intensity of the diode as a function of the applied voltage to the EOM device.

between the top contact and the SiGe layer. A n-type doping concentration of 10^{15}–10^{16} cm^{-3} is also estimated in the SiGe layer. The Schottky contact parameters have been extracted from the I–V curve, following the methods reported to the literature.[25,26] Considering a Richardson constant of 120 × 0.12 A/(cm^2 K^2),[27] an ideality factor of 1.43 is obtained, together with a Schottky barrier of 0.6 eV. Interestingly, the Schottky diode characteristic allows the characterization of the device both in injection and depletion regimes.

The total insertion loss of the 2.6-mm-length modulator has been estimated to be 4.2, 8.0, and 15.6 dB at wavelengths of 6.4, 8.5, and 10.7 μm, respectively. Different contributions have been identified. On one hand, by the characterization of a sample with similar dimensions, 4 dB/cm losses at 8.5 μm wavelength are attributed to the waveguide (without the top metal influence). This value corresponds to 1 dB loss for the 2.6 mm-length device. On the other hand, the presence of the top metal is responsible for the additional losses, taking a value of 7 dB at 8.5 μm wavelength, which is compatible with numerical simulations. This contribution has been analyzed by comparing a device with and without top metal contact.

Electro-optical Modulation. To experimentally characterize the EOM efficiency, a tunable quantum-cascade laser (QCL) in pulsed regime at 100 kHz is coupled from free-space to the waveguide by mean of a pair of ZnSe aspherical lenses in a butt coupling configuration. The output beam is then collected in a mid-IR photodetector, which signal is then amplified in lock-in system synchronized with the pulsed laser.

https://doi.org/10.1021/acsphotonics.1c01449
ACS Photonics XXXX, XXX, XXX–XXX

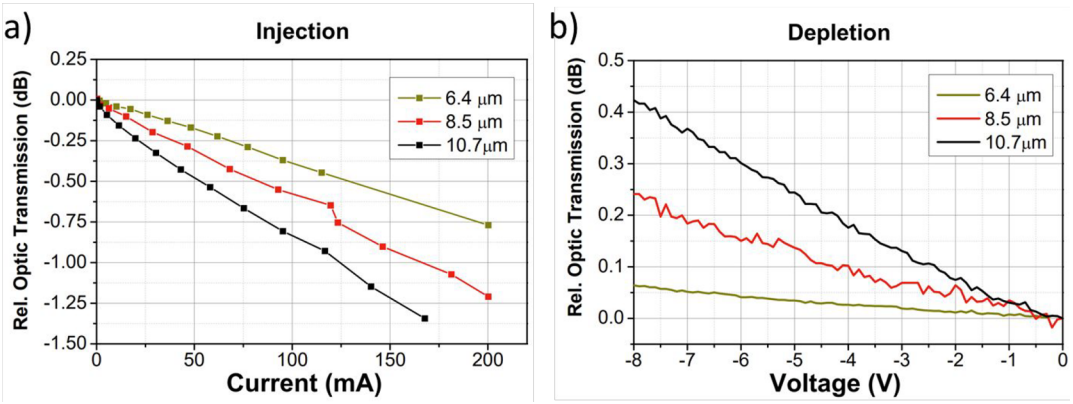

Figure 4. Static EOM transmission relative to zero bias voltage as a function of the (a) current injected to the diode and (b) applied voltage in depletion configuration. Three wavelengths are experimentally reported: 6.4, 8.5, and 10.7 μm.

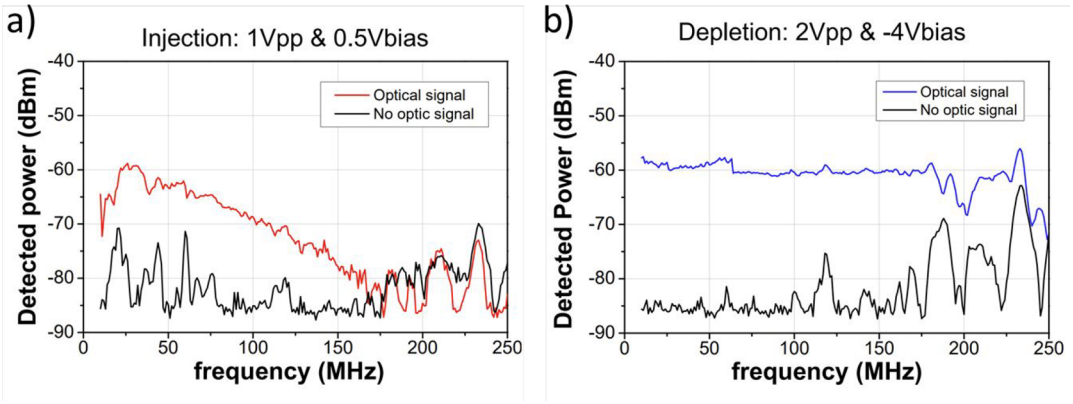

Figure 5. Amplitude of the photodetected signal as a function of the frequency in (a) carrier injection regime with 1 Vpp applied electrical signal and 0.5 V bias and (b) carrier depletion regime with 2 Vpp applied electric signal and −4 V bias. The black color represents the background noise, obtained as the detected signal when the optical beam is turned off.

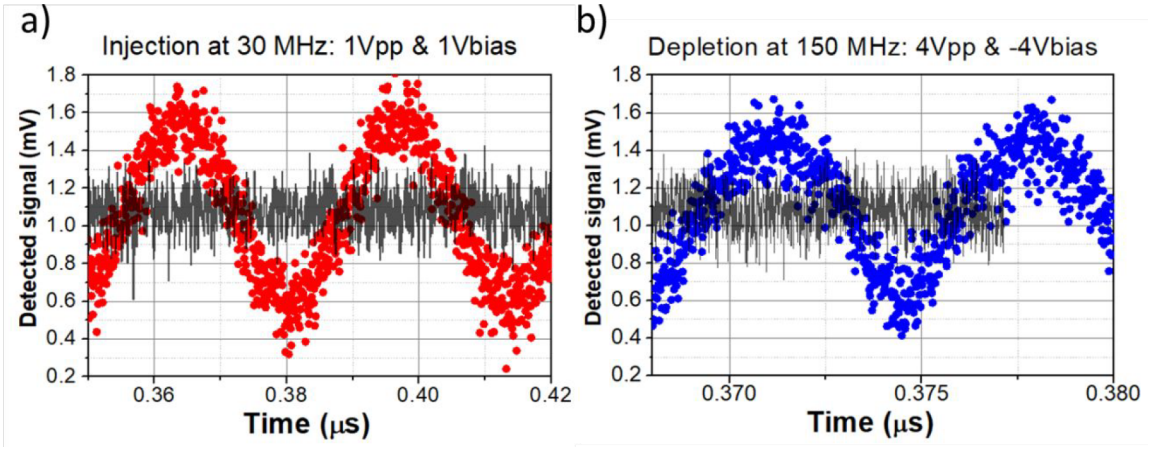

Figure 6. Photodetected signal at 8 μm wavelength in (a) carrier injection regime with 1 Vpp applied electric signal at 30 MHz and 1 V bias, and (b) carrier depletion regime with 4 Vpp electric signal at 150 MHz and −4 V bias. A similar measurement with the mid-IR source turned off is shown in black color.

Tip probes are also used to access the top and bottom electrodes.

The static optical transmission (normalized by the transmission when no voltage is applied) as a function of the current is reported in Figure 4a for different wavelengths in injection regime. As observed, the transmission decreases when the current increases, due to a carrier density increase inside the waveguide that partially absorbs the mid-IR light. Also, the modulation amplitude increases with the wavelength, confirming the higher FCPD efficiency at longer mid-IR wavelengths.[19,22] Noticeably, a maximum variation of 1.3 dB is obtained at 10.7 μm wavelength for a current of 170 mA. Noticeably, this is, to date, the largest electro-optical modulation reported on-chip at wavelengths longer than 8 μm. The optical transmission as a function of the reverse bias (depletion regime) is also reported in Figure 4b. In this case,

https://doi.org/10.1021/acsphotonics.1c01449
ACS Photonics XXXX, XXX, XXX−XXX

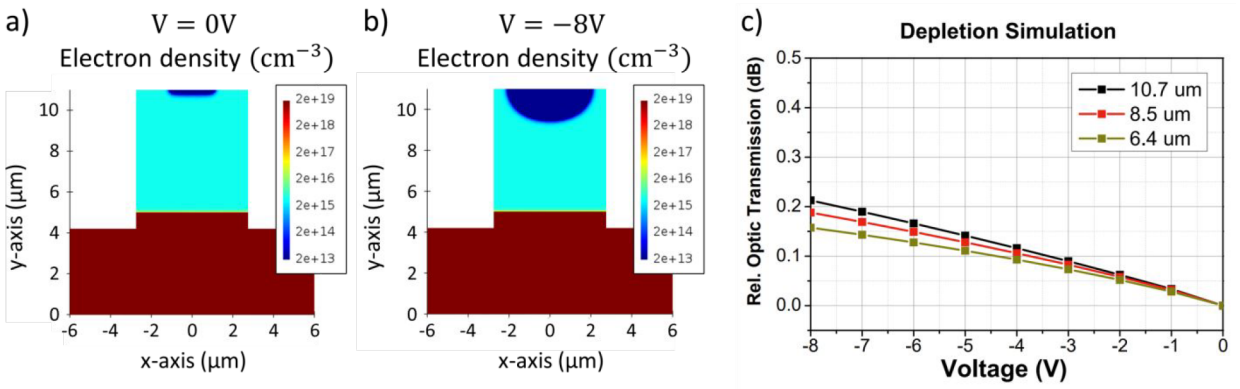

Figure 7. (a, b) Electrical simulations of the EOM structure at 0 and −8 V bias voltage. A substrate and SiGe layer electron concentration of 2×10^{19} cm^{-3} and 4×10^{15} cm^{-3} are assumed, respectively. (c) Simulated optical transmission relative to zero bias as a function of the voltage applied in depletion configuration, at 6.4, 8.5, and 10.7 μm wavelengths.

the transmission increases with the bias voltage, due to a depletion of residual carriers inside the waveguide. A maximum variation of 0.4 dB is obtained at −8 V applied to the structure.

Once the modulation efficiency has been studied, high-speed operation is also investigated by a dynamic characterization. To that end, a continuous-wave QCL at 8 μm wavelength is used. It should be noted that the EOM bandwidth does not depend on the mid-IR wavelength, but only on the diode electric features. The output optical beam is then collected and sent to a fast mid-IR detector, operating up to 600 MHz. A sinusoidal bias signal is applied to the EOM structure, and an electrical spectrum analyzer is used to measure the photodetected signal as a function of the applied bias frequency.

The dynamic characterization results are reported in Figure 5, for carrier injection and depletion configurations. In both cases, the modulated signal is compared with a noise measurement (in black), in which the laser was turned off. The high noise level is attributed to radiation from the metallic electrodes that is detected in the signal analyzer equipment, preventing an appropriate characterization at high frequency in the available experimental setup. As observed in Figure 5, a different behavior is obtained when comparing injection and depletion regimes. In injection, the amplitude of the modulation decreases almost linearly with the electrical signal frequency above 50 MHz. In contrast, the modulation amplitude in the depletion regime is flat up to 225 MHz, while the high noise level prevents a correct characterization beyond this frequency. A signal drop around 200 MHz is also attributed to the high noise level measured around this frequency.

To confirm the correct dynamic characterization of the EOM (Figure 5), the electrical signal from the photodetector is also sent to a sampling oscilloscope. As shown in Figure 6, on-chip optical modulation is clearly seen at 30 MHz and at 150 MHz in injection and depletion regimes, respectively. For this measurement the peak-to-peak voltage applied to the device is 4 V in depletion regime and 1 V injection regime.

Numerical Simulations and Analysis. To analyze these results, optical and electrical simulations of the Schottky diode are performed in depletion regime, considering a residual n-doped concentration of 4×10^{15} cm^{-3} in the graded SiGe layer and a bias voltage variation from 0 to −8 V. The increase of the depleted region in the waveguide from 0 to −8 V is clearly seen in parts a and b of Figure 7 (in dark blue color). Then, the charge profile of the EOM structure is translated to an absorption coefficient map, by using the of FCPD effect (Figure 1b). Next, this absorption map is numerically applied to the optical mode profile. Finally, the absorption variation with respect to zero bias voltage in the 2.6 mm long device is obtained. The resulting static transmission variations are reported in Figure 7c, for different values of the applied bias voltage and wavelengths used in the experiments. The general evolution of the simulated optical transmission with respect to the voltage is in relatively good agreement with the experiments.

Interestingly, this agreement between experimental and simulated results paves the way for further EOM improvements. For instance, an enhancement of the modulation efficiency and a reduction of the insertion loss are expected in future works, by tailoring the Ge-concentration profile of the platform. On one hand, specific SiGe-alloy profiles can optimize the overlap between the optical mode and the region in which the carrier concentration is modulated. On the other hand, it will be likewise possible to reduce the interaction between optical mode and the top metal contact, while keeping a low mode overlap with the Si substrate.

CONCLUSION

In summary, this work is the first experimental demonstration of an integrated electro-optic modulator that covers a wide spectrum range of the mid-IR, spanning from 6.4 to 10.7 μm wavelengths. To that end, the unique confinement features of Ge-rich graded-index SiGe platforms are exploited. On one hand, the used platform allows a broadband mode confinement on the top of the SiGe waveguide, where a carrier concentration variation is obtained with an embedded Schottky diode. On the other hand, this unique confinement also reduces the optical overlap with a highly doped Si-substrate used to provide a compact diode structure. By mean of this design, a maximal transmission modulation of 1.3 dB is remarkably obtained by carrier injection at 10.7 μm wavelength. Moreover, this work has reported carrier injection modulation at frequencies of a few tens of MHz, which can already be used for synchronous detection schemes. Noticeably, a higher frequency operation up to 225 MHz has also been demonstrated in carrier depletion configuration, only limited by the high noise of the experimental setup. Further improvements will rely on an optimization of the characterization setup and the graded SiGe layer. In this way, thanks to a provided numerical model, the optical mode confinement in

https://doi.org/10.1021/acsphotonics.1c01449
ACS Photonics XXXX, XXX, XXX−XXX

the waveguide can be engineered to optimize or minimize its overlap with the carrier distribution profiles. In conclusion, this work paves the way for the development of integrated EOM operating at high-frequency and covering a wide mid-IR spectrum range, including the long-wave regime, thus enabling exciting perspectives in a plethora of applications.

AUTHOR INFORMATION

Corresponding Author

Miguel Montesinos-Ballester − *Centre de Nanosciences et de Nanotechnologies, Université Paris-Saclay, CNRS, 91120 Palaiseau, France;* orcid.org/0000-0003-3711-3933; Email: miguel.montesinos@c2n.upsaclay.fr

Authors

Lucas Deniel − *Centre de Nanosciences et de Nanotechnologies, Université Paris-Saclay, CNRS, 91120 Palaiseau, France*

Natnicha Koompai − *Centre de Nanosciences et de Nanotechnologies, Université Paris-Saclay, CNRS, 91120 Palaiseau, France*

Thi Hao Nhi Nguyen − *Centre de Nanosciences et de Nanotechnologies, Université Paris-Saclay, CNRS, 91120 Palaiseau, France*

Jacopo Frigerio − *L-NESS, Dipartimento di Fisica, Politecnico di Milano, Polo di Como, 22100 Como, Italy*

Andrea Ballabio − *L-NESS, Dipartimento di Fisica, Politecnico di Milano, Polo di Como, 22100 Como, Italy;* orcid.org/0000-0002-2957-8717

Virginia Falcone − *L-NESS, Dipartimento di Fisica, Politecnico di Milano, Polo di Como, 22100 Como, Italy;* orcid.org/0000-0002-7560-3805

Xavier Le Roux − *Centre de Nanosciences et de Nanotechnologies, Université Paris-Saclay, CNRS, 91120 Palaiseau, France*

Carlos Alonso-Ramos − *Centre de Nanosciences et de Nanotechnologies, Université Paris-Saclay, CNRS, 91120 Palaiseau, France*

Laurent Vivien − *Centre de Nanosciences et de Nanotechnologies, Université Paris-Saclay, CNRS, 91120 Palaiseau, France;* orcid.org/0000-0002-2980-7225

Adel Bousseksou − *Centre de Nanosciences et de Nanotechnologies, Université Paris-Saclay, CNRS, 91120 Palaiseau, France*

Giovanni Isella − *L-NESS, Dipartimento di Fisica, Politecnico di Milano, Polo di Como, 22100 Como, Italy;* orcid.org/0000-0001-5951-7440

Delphine Marris-Morini − *Centre de Nanosciences et de Nanotechnologies, Université Paris-Saclay, CNRS, 91120 Palaiseau, France*

Complete contact information is available at: https://pubs.acs.org/10.1021/acsphotonics.1c01449

Author Contributions

D.M.-M. and M.M.-B. conceived the experiment and performed the simulations. M.M.-B., N.K., and X.L.R did the fabrication. M.M.-B., L.D., and N.K. did the experiments. M.M.-B. and T.T.N.N did the numerical simulations. J.F., A.B., V.F., and G.I. carried out the epitaxial growth. M.M.-B. wrote the article and discussed the results with C.A.-R., L.V., A.B., G.I., and D.M.-M.

Notes

The authors declare no competing financial interest.

ACKNOWLEDGMENTS

Fabrication engineers Jean-René Coudevylle, Etienne Herth and Cédric Villebasse are acknowledged for fabrication development contribution. L-NESS laboratory is also acknowledged for the SiGe-alloy epitaxial growth. This work was supported by ANR Light-up Project (ANR-19-CE24-0002-01). The fabrication of the device was partially performed at the Plateforme de Micro-NanoTechnologie/C2N, which is partially funded by the "Conseil Général de l'Essonne". This work was partly supported by the French RENATECH network.

REFERENCES

(1) Meade, M. L. Advances in lock-in amplifiers. *J. Phys. E Sci. Instrum* **1982**, *15*, 395.

(2) Lin, H.; Luo, Z.; Gu, T.; Kimerling, L. C.; Wada, K.; Agarwal, A.; Hu, J. Mid-infrared integrated photonics on silicon: a perspective. *Nanophotonics* **2017**, *7* (2), 393−420.

(3) Soref, R. Mid-infrared photonics in silicon and germanium. *Nat. Photonics* **2010**, *4*, 495−497.

(4) Su, Y.; Wang, W.; Hu, X.; Hu, H.; Huang, X.; Wang, Y.; Si, J.; Xie, X.; Han, B.; Feng, H.; Hao, Q.; Zhu, G.; Duan, T.; Zhao, W. 10 Gbps DPSK transmission over free-space link in the mid-infrared. *Opt. Express* **2018**, *26*, 34515−34528.

(5) Pirotta, S.; Tran, N. L.; Jollivet, A.; Biasiol, G.; Crozat, P.; Manceau, J.-M.; Bousseksou, A.; Colombelli, R. Fast amplitude modulation up to 1.5 GHz of mid-IR free-space beams at room-temperature. *Nat. Commun.* **2021**, *12*, 799.

(6) Nedeljkovic, M.; Littlejohns, C.; Khokhar, A.; Banakar, M.; Cao, W.; Penades, J.; Tran, D.; Gardes, F.; Thomson, D.; Reed, G.; Wang, H.; Mashanovich, G. Silicon-on-insulator free-carrier injection modulators for the mid-infrared. *Opt. Lett.* **2019**, *44*, 915−918.

(7) Mashanovich, G.; Nedeljkovic, M.; Soler-Penades, J.; Qu, Z.; Cao, W.; Osman, A.; Wu, Y.; Stirling, C.; Qi, Y.; Cheng, Y.; Reid, L.; Littlejohns, C.; Kang, J.; Zhao, Z.; Takenaka, M.; Li, T.; Zhou, Z.; Gardes, F.; Thomson, D.; Reed, G. Group IV mid-infrared photonics [Invited]. *Opt. Mater. Express* **2018**, *8*, 2276−2286.

(8) Marris-Morini, D.; Vakarin, V.; Ramirez, J. M.; Liu, Q.; Ballabio, A.; Frigerio, J.; Montesinos, M.; Alonso-Ramos, C.; Le Roux, X.; Serna, S.; Benedikovic, D.; Chrastina, D.; Vivien, L.; Isella, G. Germanium-based integrated photonics from near- to mid-infrared applications. *Nanophotonics* **2018**, *7*, 1781−1793.

(9) Zhang, L.; Agarwal, A.; Kimerling, L. C.; Michel, J. Nonlinear Group IV photonics based on silicon and germanium: from near-infrared to mid-infrared. *Nanophotonics* **2014**, *3*, 247−268.

(10) Malik, A.; Dwivedi, S.; Van Landschoot, L.; Muneeb, M.; Shimura, Y.; Lepage, G.; Van Campenhout, J.; Vanherle, W.; Van Opstal, T.; Loo, R.; Roelkens, G. Ge-on-Si and Ge-on-SOI thermo-optic phase shifters for the mid-infrared. *Opt. Express* **2014**, *22*, 28479−28488.

(11) Radosavljevic, D.; Radosavljević, A.; Schilling, C.; Hugger, S.; Ostendorf, R.; Kuyken, B.; Roelkens, G. Thermally Tunable Quantum Cascade Laser With an External Germanium-on-SOI Distributed Bragg Reflector. *IEEE J. S. Top. in Quantum Electron.* **2019**, *25*, 1−7.

(12) Mittal, V.; Devitt, G.; Nedeljkovic, M.; Carpenter, L.; Chong, H.; Wilkinson, J.; Mahajan, S.; Mashanovich, G. Ge on Si waveguide mid-infrared absorption spectroscopy of proteins and their aggregates. *Biomed. Opt. Express* **2020**, *11*, 4714−4722.

(13) Kozak, D.; Tyndall, N.; Pruessner, M.; Rabinovich, W.; Stievater, T. Germanium-on-silicon waveguides for long-wave integrated photonics: ring resonance and thermo-optics. *Opt. Express* **2021**, *29*, 15443−15451.

(14) Sinobad, M.; Monat, C.; Luther-Davies, B.; Ma, P.; Madden, S.; Moss, D.; Mitchell, A.; Allioux, D.; Orobtchouk, R.; Boutami, S.; Hartmann, J.; Fedeli, J.; Grillet, C. Mid-infrared octave spanning supercontinuum generation to 8.5 μm in silicon-germanium waveguides. *Optica* **2018**, *5*, 360−366.

(15) Montesinos-Ballester, M.; Liu, Q.; Vakarin, V.; Ramirez, J. M.; Alonso-Ramos, C.; Le Roux, X.; Frigerio, J.; Ballabio, A.; Talamas, E.; Vivien, L.; Isella, G.; Marris-Morini, D. On-chip Fourier-transform spectrometer based on spatial heterodyning tuned by thermo-optic effect. *Sci. Rep.* **2019**, *9*, 14633.
(16) Ho, C.; Zhao, Z.; Li, Q.; Takagi, S.; Takenaka, M. Mid-infrared tunable Vernier filter on a germanium-on-insulator photonic platform. *Opt. Lett.* **2019**, *44*, 2779−2782.
(17) Sánchez-Postigo, A.; Ortega-Moñux, A.; Soler Penadés, J.; Osman, A.; Nedeljkovic, M.; Qu, Z.; Wu, Y.; Molina-Fernández, Í.; Cheben, P.; Mashanovich, G.; Wangüemert-Pérez, J. Suspended germanium waveguides with subwavelength-grating metamaterial cladding for the mid-infrared band. *Opt. Express* **2021**, *29*, 16867−16878.
(18) Li, T.; Nedeljkovic, M.; Hattasan, N.; Cao, W.; Qu, Z.; Littlejohns, C.; Penades, J.; Mastronardi, L.; Mittal, V.; Benedikovic, D.; Thomson, D.; Gardes, F.; Wu, H.; Zhou, Z.; Mashanovich, G. Ge-on-Si modulators operating at mid-infrared wavelengths up to 8 μm. *Photon. Res.* **2019**, *7*, 828−836.
(19) Montesinos-Ballester, M.; Vakarin, V.; Ramirez, J. M.; Liu, Q.; Alonso-Ramos, C.; Le Roux, X.; Frigerio, J.; Ballabio, A.; Barzaghi, A.; Deniel, L.; Bouville, D.; Vivien, L.; Isella, G.; Marris-Morini, D. Optical modulation in Ge-rich SiGe waveguides in the mid-infrared wavelength range up to 11 μm. *Commun. Mater.* **2020**, *1*, 6.
(20) Montesinos-Ballester, M.; Lafforgue, C.; Frigerio, J.; Ballabio, A.; Vakarin, V.; Liu, Q.; Ramirez, J. M.; Le Roux, X.; Bouville, D.; Barzaghi, A.; Alonso-Ramos, C.; Vivien, L.; Isella, G.; Marris-Morini, D. On-Chip Mid-Infrared Supercontinuum Generation from 3 to 13 μm Wavelength. *ACS Photonics* **2020**, *7*, 3423−3429.
(21) Ramirez, J. M.; Liu, Q.; Vakarin, V.; Frigerio, J.; Ballabio, A.; Le Roux, X.; Bouville, D.; Vivien, L.; Isella, G.; Marris-Morini, D. Graded SiGe waveguides with broadband low-loss propagation in the mid infrared. *Opt. Express* **2018**, *26*, 870−877.
(22) Nedeljkovic, M.; Soref, R.; Mashanovich, G. Z. Predictions of Free-Carrier Electroabsorption and Electrorefraction in Germanium. *IEEE Photonics Journal* **2015**, *7*, 1−14.
(23) Rosenblad, C.; Deller, H. R.; Dommann, A.; Meyer, T.; Schroeter, P.; von Känel, H. Silicon epitaxy by low-energy plasma enhanced chemical vapor deposition. *J. Vac. Sci. Technol. A* **1998**, *16*, 2785−2790.
(24) Golan, G.; Axelevitch, A.; Gorenstein, B.; Manevych, V. Hot-Probe method for evaluation of impurities concentration in semiconductor. *Microelectronics Journal* **2006**, *37*, 910−915.
(25) Lien, C.-D.; So, F. C. T.; Nicolet, M.-A. An improved forward I-V method for nonideal Schottky diodes with high series resistance. *IEEE Trans. Electron Devices* **1984**, *31*, 1502−1503.
(26) Sze, S. M. *Physics of Semiconductor Devices*; Wiley-Intersicence: 1969.
(27) Crowell, C. R. Richardson constant and tunneling effective mass for thermionic and thermionic-field emission in Schottky barrier diodes. *Solid-State Electron.* **1969**, *12*, 55−59.

https://doi.org/10.1021/acsphotonics.1c01449
ACS Photonics XXXX, XXX, XXX−XXX